92-GT-58

THE AMERICAN SOCIETY OF MECHANICAL ENGINEERS
345 E. 47 St., New York, N.Y. 10017

A Wide-Range Axial-Flow Compressor Stage Performance Model

GREGORY S. BLOCH*
Mechanical Engineering Department
WALTER F. O'BRIEN
College of Engineering
Virginia Polytechnic Institute and State University

ABSTRACT

Dynamic compression system response is a major concern in the operability of aircraft gas turbine engines. Multi-stage compression system computer models have been developed to predict compressor response to changing operating conditions. These models require a knowledge of the wide-range, steady-state operating characteristics as inputs, which has limited their use as predicting tools.

The full range of dynamic axial-flow compressor operation spans forward and reversed flow conditions. A model for predicting the wide flow range characteristics of axial-flow compressor stages was developed and applied to a 3-stage, low-speed compressor with very favorable results and to a 10-stage, high-speed compressor with mixed results.

Conclusions were made regarding the inception of stall and the effects associated with operating a stage in a multistage environment. It was also concluded that there are operating points of an isolated compressor stage that are not attainable when that stage is operated in a multi-stage environment.

NOMENCLATURE

A	Area
c	Blade chord
c_p	Specific heat
D_{eq}	Equivalent diffusion ratio
H	Blade span
H_2	Blade wake form factor
i	Blade incidence angle
IGV	Inlet guide vane
M	Mach number
$\dot{m}$	Mass flow rate
P	Pressure
PR	Total pressure ratio
T	Temperature
TR	Total temperature ratio
U	Compressor wheel speed
V	Absolute velocity
W	Relative velocity

Greek Symbols

α	Absolute flow angle, or Angle of attack
β	Relative flow angle
β'	Blade metal angle
ϕ	Stage flow coefficient
δ	Flow deviation angle
γ	Blade stagger angle, or Ratio of specific heats
η	Stage isentropic efficiency
σ	Blade solidity
ρ	Fluid density
θ	Blade camber
θ^*	Wake momentum thickness
$\overline{\omega}$	Total pressure loss coefficient
ψ^P	Stage pressure coefficient
ψ^T	Stage temperature coefficient

Subscripts

a	Annulus
p	Profile
R	Rotor
S	Stator
s	Secondary
x	Axial direction
0	Total property
1	Rotor or stage inlet
2	Rotor or stage exit

* Current Address: Aero Propulsion and Power Directorate, Wright-Patterson AFB, OH

Presented at the International Gas Turbine and Aeroengine Congress and Exposition
Cologne, Germany June 1-4, 1992

INTRODUCTION

Mathematical models have been developed to predict dynamic compression system response to changes in inlet conditions, requests for acceleration and deceleration, and other inputs. Applications of these mathematical models (Boyer and O'Brien, 1989; Dowler, et al., 1989) have demonstrated that the models can be useful tools in the study of time-dependent compressor operation, including (but not limited to) stall and surge. The successes demonstrated by these compressor modeling capabilities have established the possibility of incorporating the models into compressor design and test programs.

The steady-state pressure and temperature characteristics for the compressor are necessary inputs to present dynamic performance models. Because the time scale of an engine transient is of the order of several seconds and the residence time for a fluid element in a compressor is of the order of 0.01 seconds, the dynamic performance is usually calculated from the steady-state characteristics with a time lag appropriately applied.

In the simplest case, the model may represent a lumped compression system and treat the pressure-rise process as incompressible (Greitzer, 1976). Depending upon the range of flows to be modeled, the required pressure-mass flow relationship may include only unstalled performance (pre-stall characteristic), or may include the in-stall and reversed-flow regimes (full-range characteristic).

A detailed, stage-by-stage model (Davis, 1986) will require individual stage characteristics. If the effects of compressibility are to be included, temperature characteristics are also required. Fig. 1 shows the general shape of full-range compressor stage pressure and temperature characteristics. Overall compression system characteristics are of similar form.

Full-range compressor and compressor stage characteristics have been obtained at least partially from experiment for the unstalled and in-stall regimes; the reversed-flow characteristics have been "backed out" using surge data, but sparse surge data and the unavailability of proper instrumentation limit the usefulness of this technique. Experimentally obtained characteristics have been used by many investigators as inputs to dynamic compression system and engine models (Saravanamuttoo, 1970; Seldner, et al., 1972; Kimzey, 1977). These models showed very good agreement with the measured dynamic response, but used actual measured data as inputs. Application of a stage-by-stage model (Davis, 1986) to a 3-stage, low-speed compressor used stage pressure characteristics published by Gamache (1985), but the stage temperature characteristics had to be synthesized as a total temperature ratio based on the overall torque coefficient. Application of this same model to a 9-stage, high-speed compressor required in-stall performance estimates based on the overall shape suggested by low-speed compressor tests. In all cases, the authors concluded that the accurate knowledge of the steady characteristics was required to obtain the desired agreement.

Current dynamic compression system models require an *a priori* knowledge of the steady-state stage characteristics for accurate prediction of dynamic response, which limits the application of these models as predictive tools. Due to the high cost of testing an actual compressor, it is desirable to predict the compression system performance from geometry. In the case of high-speed, multi-stage compressors, the power requirements to operate the rig in reversed flow and the danger of overheating at very low mass flows are sufficient to prevent testing in these flow regimes. This emphasizes the need to accurately predict full-range stage characteristics from geometry.

The present paper puts forth a model using theoretical and empirical methods for the prediction of full-range stage characteristics. A computer program was developed from the model and predictions are compared with experiment.

MODEL THEORY

The elementary axial-flow compressor stage mean-line analysis principles for forward, unstalled flow are well-known. This type of analysis assumes incompressible, inviscid flow through a single stage and uses empirical correlations to estimate the pressure losses

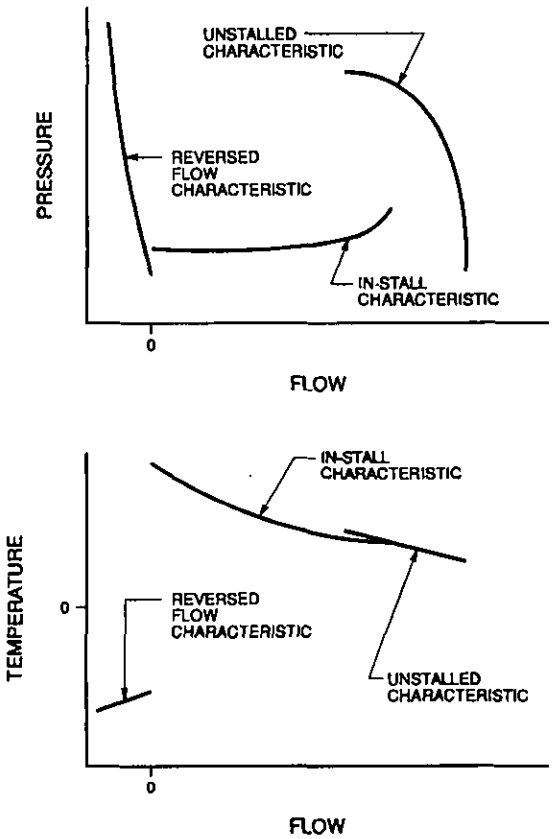

Fig. 1 Full-Range Compressor Stage Characteristic

and flow deviation in each blade row. The classical correlations are given by Lieblein (1959) and Carter (Horlock, 1973), respectively, for unstalled operation. Methods for prediction of in-stall and reversed-flow stage performance have not previously been developed.

Unstalled Forward Flow

A typical compressor stage and the flow angles associated with forward flow are shown in Fig. 2. Using the moment of momentum equation for this geometry, Euler's turbine equation gives the stage temperature rise.

$$\frac{\Delta T_0}{T_{01}} = \frac{T_{02} - T_{01}}{T_{01}} = \frac{U^2}{c_p T_{01}}\left[1 - \frac{V_{x1}}{U}\left(\frac{V_{x2}}{V_{x1}}\tan\beta_2 + \tan\alpha_1\right)\right] \qquad (1)$$

For incompressible flow, the total pressure rise for the stage is related to the total temperature rise and the blade row pressure losses by

$$P_{02} - P_{01} = \rho c_p \Delta T_0 - \left(\Delta P_{0R} + \Delta P_{0S}\right) \qquad (2)$$

For incompressible flow, the total pressure losses are related to the cascade loss parameters by

$$\bar{\omega}_R = \frac{\Delta P_{0R}}{\rho W_1^2/2} \qquad \text{and} \qquad \bar{\omega}_S = \frac{\Delta P_{0S}}{\rho V_2^2/2} \qquad (3)$$

For incompressible flow, the stage efficiency is given by

$$\eta = 1 - \frac{\Delta P_{0R} + \Delta P_{0S}}{\rho c_p \Delta T_0} \qquad (4)$$

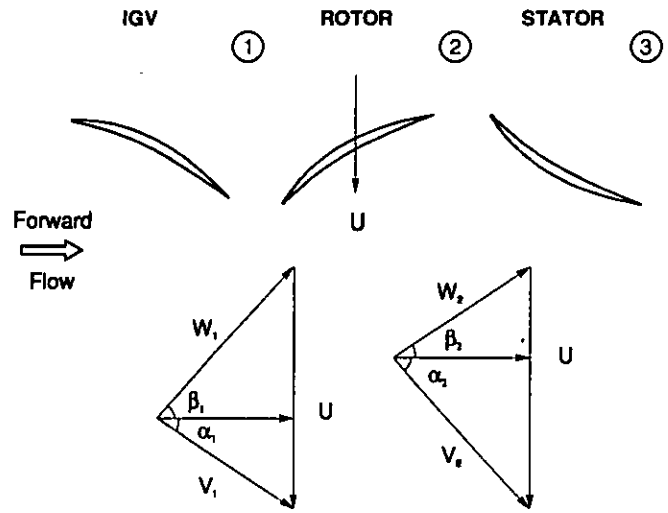

Fig. 2 Mean Radius Section of a Compressor Stage in Forward Flow Operation

Since the angles in Equation (1) are flow angles and the pressure losses cannot be calculated directly, approximations for the deviation angle and loss coefficients must be made.

To estimate the flow exit angle in the unstalled, forward flow regime, the model uses Carter's correlation (Horlock, 1973), which is for near-design operation. Because the deviation does not change significantly until the blade stalls, this angle is assumed to be constant.

$$\beta_2 - \beta_2' = \frac{m\theta}{\sqrt{\sigma}} \tag{5}$$

where m is obtained from the reference.

The blade losses are calculated as the sum of profile, annulus and secondary losses. The profile losses are given by Lieblein (1959) and the annulus and secondary losses are given by Dixon (1975) as follows.

$$\bar{\omega}_p = 2\sigma \frac{\cos^2\beta_1}{\cos^3\beta_2}\left(\frac{\theta^*}{c}\right)_2 \left\{ \frac{\frac{2H_2}{3H_2 - 1}}{\left[1 - \left(\frac{\theta^*}{c}\right)_2 \frac{\sigma H_2}{\cos\beta_2}\right]^3} \right\} \tag{6}$$

$$\bar{\omega}_a = 0.02\sigma\left(\frac{c}{H}\right)\frac{\cos^2\beta_1}{\cos^3\beta_m} \tag{7}$$

$$\bar{\omega}_s = \frac{0.072}{\sigma}\frac{\cos^2\beta_1}{\cos\beta_m}\left(\tan\beta_1 - \tan\beta_2\right)^2 \tag{8}$$

where $$\tan\beta_m = \frac{\left(\tan\beta_1 + \tan\beta_2\right)}{2}$$

Stalled Forward Flow

For in-stall, forward flow operation, the flow is assumed to separate from the blade leading edge, as shown in Fig. 3, and the approximation of Moses and Thomason (1986) is used to predict the fully mixed flow angle and loss coefficient. The determination of the jet exit angle, β_2, is based on some additional empiricism and is discussed later. The jet velocity ratio is given by

$$\frac{V_2}{V_1} = \frac{-b \pm \sqrt{b^2 - 4ac}}{2a} \tag{9}$$

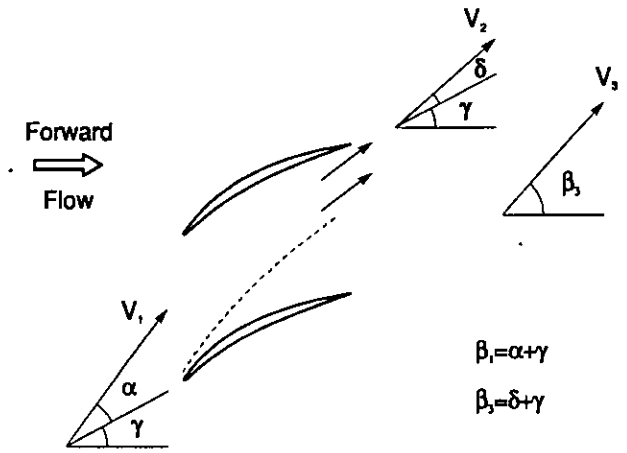

Fig. 3 Compressor Cascade Geometry and Nomenclature for Stalled Operation

where

$$a = 1 + \frac{0.15\sigma}{\cos\beta_1} \qquad b = \frac{-2\cos\beta_1\cos\delta}{\cos\gamma} \qquad c = \frac{2\cos\beta_1\cos\alpha}{\cos\gamma} - 1$$

To give meaningful results, only the positive result in Equation (9) is used.

The fully mixed flow angle and loss coefficient are given by

$$\tan\beta_3 = \frac{V_2\sin\beta_2}{V_1\cos\beta_1} \tag{10}$$

$$\bar{\omega} = \frac{P_{01} - P_{03}}{\rho V_1^2/2}$$

$$= \left(1 + \frac{0.15\sigma}{\cos\beta_1}\right)\frac{V_2^2}{V_1^2} + 2\cos\beta_1\left(\cos\beta_1 - \frac{V_2}{V_1}\cos\beta_2\right) - \frac{\cos^2\beta_1}{\cos^2\beta_3} \tag{11}$$

Because the profile losses for a stalled blade row are much larger than the annulus and secondary losses, the latter are ignored in this flow regime.

Reversed Flow

A typical compressor stage and the flow angles associated with reversed flow are shown in Fig. 4. The development of the basic stage performance equations is a direct extension of that presented previously, with the subscripts changed to reflect the direction of flow. Using the moment of momentum equation for this geometry, Euler's turbine equation gives the stage temperature rise.

$$\frac{\Delta T_0}{T_{02}} = \frac{T_{02} - T_{01}}{T_{02}} = \frac{-U^2}{c_p T_{02}}\left[1 - \frac{V_{x1}}{U}\left(\frac{V_{x2}}{V_{x1}}\tan\alpha_2 + \tan\beta_1\right)\right] \tag{12}$$

It should be noted that the compressor does work on the fluid in the direction of flow, increasing its temperature in that direction. When the compressor is operating in reversed flow, the temperature at station 1 is greater than at station 2 and the result in Equation (12) is negative. The flow angle, β_1, is assumed to be the blade metal angle as suggested by Turner and Sparkes (1964) and by Koff and Greitzer (1986).

For incompressible flow in the reversed direction, the pressure losses are *added* in Equation 13 because they are positive in the direction of flow, which is from station 2 to station 1.

$$P_{02} - P_{01} = \rho c_p \Delta T_0 + \left(\Delta P_{0R} + \Delta P_{0S}\right) \tag{13}$$

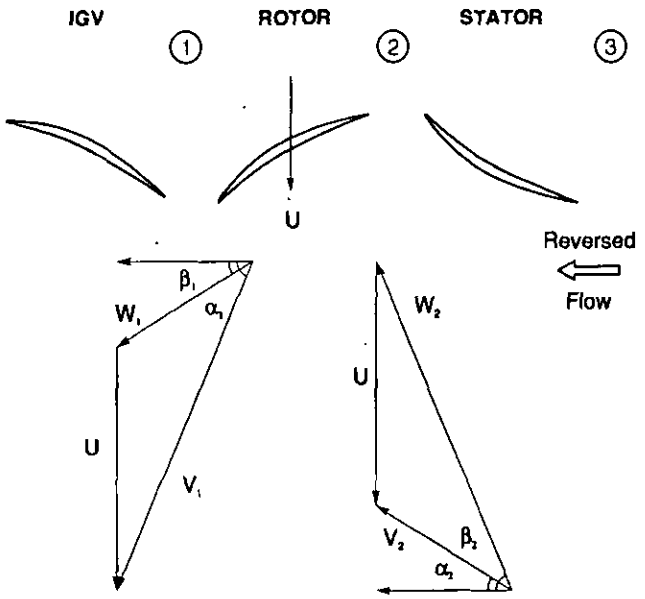

Fig. 4 Mean Radius Section of a Compressor Stage in Reversed-flow Operation

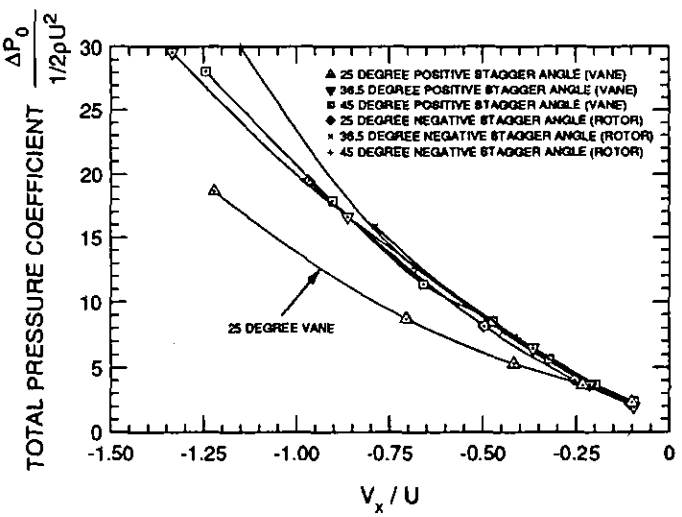

Fig. 5 Corrected Pressure Losses in a Reversed-flow Compressor Cascade

In a cascade experiment to study reversed flow, Carneal (1990) showed that losses in the reversed-flow region, when non-dimensionalized by wheel speed, collapse onto a single parabola as shown in Fig. 5. While the data for reversed-flow losses were derived from cascade tests, it is possible to express the results in terms of wheel speed for a rotating cascade. The method is shown in Appendix A. Although the loss curve for one stagger angle diverges from the others at reversed flow coefficients less than -0.25, the region of typical compressor operation is $V_x/U \geq -0.25$, even during a deep surge cycle. The implication of this result is that the reversed-flow losses are reasonably approximated as a function of mass flow only, independent of flow angle, solidity, blade shape, and other flow details. A parabola fit to the five coincident curves of Carneal's data is used to determine the blade row losses as a function of mass flow at the rotor inlet (station 2 in Fig. 4); the same value is then used for both rotor and stator in Equation (13) to calculate the stage pressure rise.

Gamache (1985) noted that the last stage stator in reversed flow functions in the same manner as the IGV during forward flow. The flow enters the blade row with a small angle of attack and is turned from the axial direction, accelerating the flow like a nozzle. Gamache measured a negligible pressure loss across this blade row in reversed-flow operation, so the model neglects the losses for the last stator of the compressor when operating in reversed flow.

The stage efficiency is not a meaningful number in reversed flow because the large pressure losses in the reversed flow analog of Equation (4) and the use of correction factors discussed in a later section often make the result fall outside of the bounds of $0 \leq \eta \leq 1$.

EMPIRICAL OBSERVATIONS AND ADDITIONS

Although the present model is based on fundamental fluid mechanics and experiments, some empirical additions have been necessary to achieve the desired agreement with measured characteristics. These additions were based on logical extensions of the published literature.

Criteria Used For Stall Inception

Yocum (1988) reported the angle of incidence at which flow separation would occur in a test cascade to be 8°. Longley and Hynes (1990) reported that a stage operating as part of a multistage compressor can remain unstalled at flows much lower than the isolated clean-flow stall point. It has been suggested by Cousins (1991) that the pumping action of the downstream stages tends to prevent upstream flow separation. In an attempt to model this effect, the angle of incidence at which separation occurs is assumed to be the sum of the isolated stall incidence (8°) and a correction for the location of the stage in a multistage environment, which leads to the following expression for stalling incidence.

$$i_{stall} = 8° + a\Delta i \tag{14}$$

where $a = \dfrac{current\ stage\# - 1}{total\ \#\ stages - 1}$ $\qquad \Delta i = i_{\substack{first\ stage \\ stall}} - 8°$

The value used for the first stage stalling incidence was obtained from the first stage of the 3-stage compressor tested by Gamache (1985), which stalled at 16° angle of incidence. If it is assumed that this result is generally applicable, the bounds on the incidence angle for separation are $8° \leq i_{stall} \leq 16°$, with 8° used for the last stage and 16° used for the first stage of a modeled compressor. This correlation was applied to all stages modeled and reported in this paper.

When a blade row stalls, the flow at the trailing edge consists of a high velocity jet near the pressure surface and a separated, recirculating region near the suction surface. It is expected that the wake will not have sufficient time to mix to a uniform condition before reaching the downstream blade row and that the recirculating region will be sufficient to initiate stall of the downstream row. For this reason, the model assumes that when the rotor stalls, the downstream stator stalls as well.

Stalled-Flow Jet Exit Angle

The reasoning used to determine the stalled flow jet exit angle is similar to that presented in the previous section. The approximation of Moses and Thomason (1986) suggests that the flow leaves the trailing edge at approximately the stagger angle. The present authors suggest that the pumping action of the downstream stages, which delays the onset of stall in the upstream stages, tends to reduce the extent of separation once stall occurs.

The jet angle is assumed to be the sum of the trailing edge blade angle and a correction for the location of the stage in a multistage environment, which suggests the following correlation for the jet exit angle.

$$\beta_2 = \beta_2' + a(\beta_1' - \gamma) \tag{15}$$

where $a = \dfrac{current\ stage\# - 1}{total\ \#\ stages - 1}$

The resulting bounds on the exit jet angle are $\beta_1' \le \beta_2 \le \gamma$, with the lower bound of β_1' being used for the first stage and γ for the last stage. This correlation was applied to all stages modeled and reported in this thesis.

Recovery Hysteresis

It is well-known (Graham and Guentert, 1965) that a compressor will not recover from stall until the mass flow is increased to a value greater than that which existed when stall was initiated, but the extent of the hysteresis that will be present is not well understood. The present model predicts the stage performance in the region where the characteristics are double valued, but does not attempt to calculate the extent of the hysteresis. To include this effect in the model, the stalled flow calculations are begun with an incidence of 6° before stall inception. This selected amount of hysteresis is considered reasonable based on experience of the authors, but cannot be calculated by any present theory. Because the stalled calculations involve solving the quadratic in Equation (9), solution is not possible for all incidence angles and not all of the predicted stage characteristics to be presented show the full 6° of hysteresis.

Reversed-Flow Pressure Prediction

The flow field in a compressor operating in annulus reversed flow is not well understood, as there has been little research performed in this flow regime. The present model predicts reversed-flow performance with reference to the experiments of Carneal (1990) and Equation (13), with an empirical correction in the fonn of Equation (16) to improve agreement with experiments.

$$P_{02} - P_{01} = a_1 \rho c_p \Delta T_0 + a_2 \left(\Delta P_{0R} + \Delta P_{0S} \right) + a_3 \qquad (16)$$

where $a_1 = 0.31$

$a_2 = 1.33$

$a_3 = 0.20$

By use of the performance of the first stage of the compressor tested by Gamache (1985), the values for the coefficients in the above equation were obtained and were used in all predictions presented. It should be noted that at this time there is no theory to predict these coefficients.

ASSEMBLY INTO A WIDE RANGE PREDICTION MODEL

A full-range stage performance computer model (FULRANGE) was developed as an assembly of the methods discussed in the previous sections. To implement the model over the range of mass flow coefficients in the forward flow regime, the relative flow angle at the rotor inlet is varied from zero angle of attack to zero flow (relative flow angle is 90°) in one degree increments and the appropriate flow calculation is applied. To generate the reversed-flow characteristics, the model increments the mass flow index, V_x/U, by a fixed (negative) amount and the reversed-flow calculations are performed.

The information required by the model to predict stage performance is the rotor and stator mean-radius geometry, as summarized in Table 1.

APPLICATION TO A LOW SPEED COMPRESSOR

To verify the accuracy of the FULRANGE technique, the model was used to predict the performance of the low-speed 3-stage rig tested by Gamache (1985). This compressor had a constant flowpath annulus with 3 non-repeating stages; further details about this compressor can be found in the reference. For this machine, a stage was defined as a rotor and the downstream stator.

rotor blade leading edge angle
rotor blade trailing edge angle
rotor blade stagger angle
rotor blade mean radius
number of rotor blades
rotor blade chord
rotor blade span
rotor blade thickness/chord ratio
IGV or (upstream) stator exit flow angle
stator blade leading edge angle
stator blade trailing edge angle
stator blade stagger angle
stator blade mean radius
number of stator blades
stator blade chord
stator blade span
stator blade thickness/chord ratio
stage axial velocity ratio
location (stage number) of stage being modeled
number of stages in the machine being modeled

Table 1 FULRANGE Model Input Parameters

The predicted and measured pressure characteristics for this machine are presented in Figs. 6 through 8. The predicted characteristics showed very good qualitative agreement in the forward flow region and excellent agreement in the reversed-flow region. The prediction has the same curvature as the measured characteristic throughout the entire flow regime and has no unexplained discontinuities.

For all 3 stages of this machine, the FULRANGE model predicted the flow coefficient, V_x/U, for transition to abrupt stall within 0.01 of the measured value. It should be noted that this difference between predicted and measured transition represents an error of less than 1° angle of incidence to the rotor.

The unstalled pressure prediction was within 0.15 of the measured values for the first and third stages, but the second stage agreement was not as good. The unstalled prediction for the second stage was within 0.20 of the measured values.

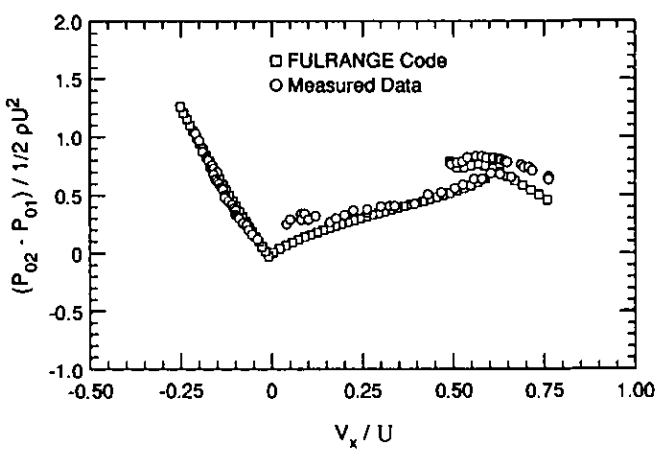

Fig. 6 3-Stage Test Compressor First Stage Pressure Characteristic

For flow coefficients greater than 0.10, approximately 90% of the in-stall data were within 0.10 of the predicted pressure characteristic. The general shape of the predicted characteristic is the same for all stages, reaching a zero pressure rise at zero flow, while many compressors exhibit some positive pressure rise at zero flow. The mechanisms for this observed phenomenon are not currently understood.

The first stage reversed-flow pressure prediction is coincident with the measured characteristic, as would be expected (this was the one stage used to develop the correlation coefficients). Application of the reversed-flow model to the second stage prediction yielded an essentially exact match to the characteristic. This supports the application of the results of Carneal (1990), which indicated that both rotors and stators in reversed flow could be treated as nearly equal loss producers. For both of these stages, the slope of the characteristic is very steep. This is because the blade row losses in reversed flow are very large as shown in Fig. 5, and a large pressure is required at station 3 as shown in Fig. 4, to force air through the stage.

The reversed-flow pressure prediction for the third stage is within 0.07 of the corresponding measured values. The more nearly horizontal characteristic for this stage is the result of the last stator in reversed flow operating in the same manner as the IGV in forward flow. Because there are small pressure losses in the last stator row (as compared to the first two stator rows), a smaller pressure at the stage exit will force flow backwards through this stage.

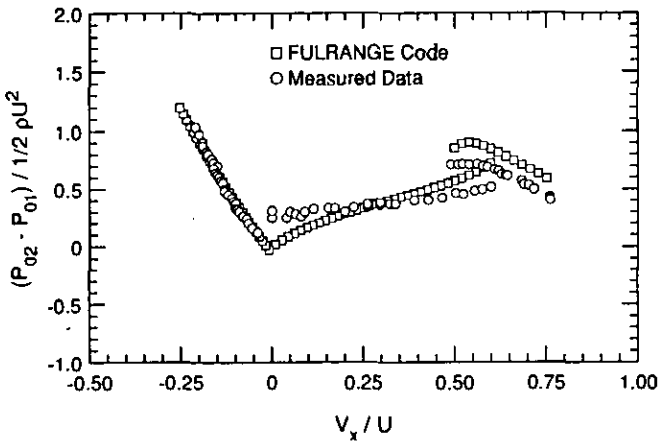

Fig. 7 3-Stage Test Compressor Second Stage Pressure Characteristic

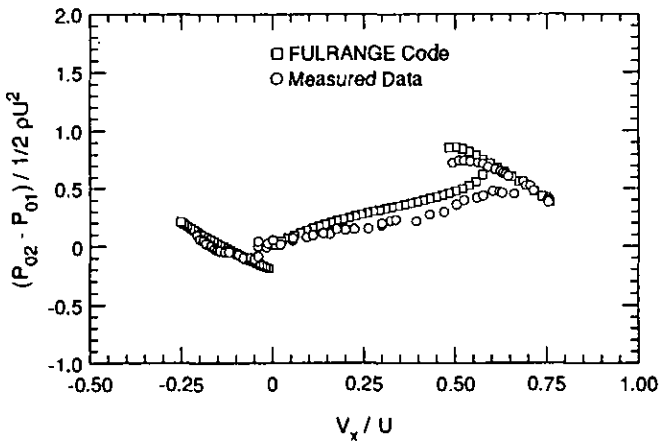

Fig. 8 3-Stage Test Compressor Third Stage Pressure Characteristic

APPLICATION TO A HIGH SPEED COMPRESSOR

The *FULRANGE* code was used to model the performance of the 10-stage, high-speed compressor tested by Copenhaver (1988). This compressor was the high pressure compressor from a modern high-performance aircraft gas turbine engine and was tested at five speeds ranging from 49.8% to 78.5% of design corrected speed to investigate stalling and recovery behavior. For this range of corrected speeds, the variable vane schedule was fixed so there was no change in stage geometry; the vanes open only at higher corrected speeds. Because the present model assumes incompressible flow across a single stage, the predicted stage characteristics are independent of wheel speed and the measured data are presented without distinction of the speed at which they were obtained. The flow, pressure, and temperature coefficients plotted in these figures are defined as follows.

$$\phi = \frac{\left[\frac{\dot{m}\sqrt{T_0}}{P_0 A}\right][\mathrm{NC}]}{0.5318} \tag{17}$$

$$\psi^P = \left[\mathrm{PR}^{\frac{\gamma-1}{\gamma}} - 1\right][\mathrm{NC}]^2 \tag{18}$$

$$\psi^T = [\mathrm{TR} - 1][\mathrm{NC}]^2 \tag{19}$$

where $[\mathrm{NC}] = \left[\frac{\left(\frac{N}{\sqrt{\theta}}\right)_{design}}{\left(\frac{N}{\sqrt{\theta}}\right)_{actual}}\right]$ and $\theta = \frac{T_0}{T_{ref}}$

Before discussing the pressure and temperature characteristics, a comment regarding the flow coefficient predictions is in order. The model predicted the transition to stall within 2° angle of incidence to the rotor for all stages in the compressor. It is unknown whether this is the result of an underlying mechanism that is approximated but not yet understood, or whether this is a fortuitous coincidence.

Pressure Characteristic Predictions

The model consistently over-predicted the unstalled pressure coefficients for the first three stages by a significant amount, as shown in Figs. 9 and 10. The second stage characteristics are similar to those of the third stage and were omitted for brevity. The reasons for the significant disagreement in this area are not clearly understood at this time, but two theories are put forth.

For the low corrected speeds at which this compressor was tested, the IGV and first two stator rows were fully closed (large stagger angles, as measured from an axial reference). Under these conditions, the flow into the IGV is at a large angle of incidence and is turned significantly away from the axial direction. The large incidence is likely to cause separation from the IGV leading edge, causing large pressure losses and a large flow deviation angle. This situation is far from design-point IGV operation and the current model is unable to approximate the performance accurately. It is believed that a similar flow separation may occur in the stator rows of stages two and three, as well.

A second effect of the closed vanes is that the flow is accelerated significantly due to the reduction in apparent flow area. This area ratio is of sufficient magnitude to cause choking of the flow (even at moderately low mass flow), a phenomenon which the present (incompressible) model is not capable of predicting.

Based on the nearly vertical pressure characteristics for the second stage (not shown) and the third stage (Fig. 10). Copenhaver (1988) concluded that choking existed in these stages. Because these stages appeared choked at high flow coefficients, and

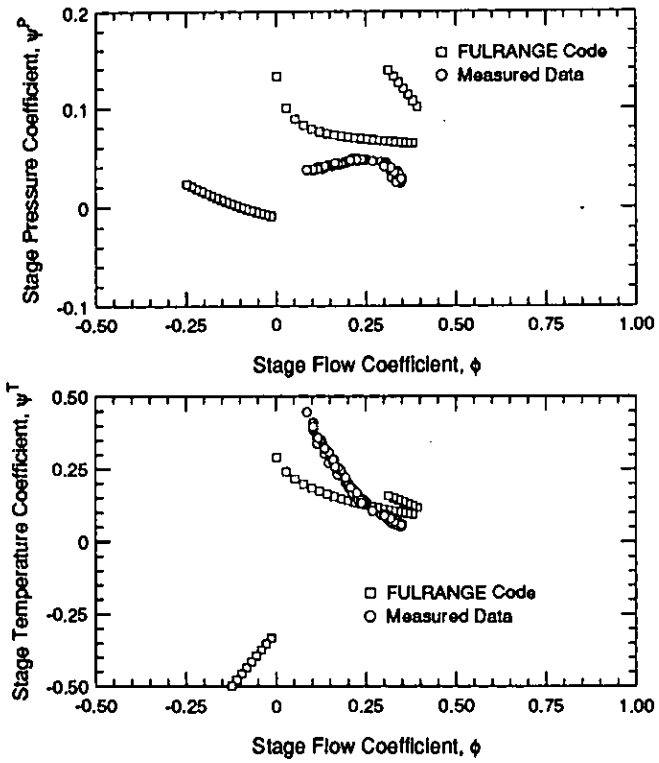

Fig. 9 10-Stage Compressor: a) First Stage Pressure Characteristic; b) First Stage Temperature Characteristic

because of the negatively sloped pressure characteristics for the entire operating region, Copenhaver concluded that they were operating in a high-flow manner under all conditions. Based on the flow angles calculated by the FULRANGE model, the present authors suggest that the stages were operating in-stall when the mass flow was low enough to eliminate the choking. The fact that there is good agreement between the predicted in-stall pressure rise and the measured performance for the second and third stages would tend to support this suggestion.

The predicted and measured pressure performance of stages four through eight are very similar and the fifth stage characterisiics shown in Fig. 11 are representative. The unstalled pressure predictions for these stages are nearly coincident with the actual data points. The in-stall predictions have the same slope and curvature as the measured characteristics, but are significantly lower in magnitude. It is believed that the under-prediction is a result of the modeling assumption of axisymmetrically stalled flow. Continuing work is addressing methods for improved modeling of the circumferential variations which exist in in-stall flows.

The qualitative agreement of the predicted and measured performance of the ninth stage is somewhat of a transition between that of the eighth and the tenth stages, and comparison is omitted for brevity.

Before discussing the operation of the tenth stage, it is instructive to look at the effect of density variation on stage performance. Under low speed conditions, the density increase across each stage is lower than the design value. The area reduction found in high speed, multi-stage compressors results in high axial velocities in the rear stages and can lead to choking.

The unstalled pressure prediction for the tenth stage agrees well with the measured data for flow coefficients less than 0.60, as shown in Fig. 12. At higher mass flows, the high velocity air at the stage entrance causes the pressure to *drop* and the stage performs like a turbine. When operated in-stall, the tenth stage was extracting work from the flow for all data points, with an apparent choking condition at a flow coefficient of 0.57. For these reasons, the predicted and measured performance were not close.

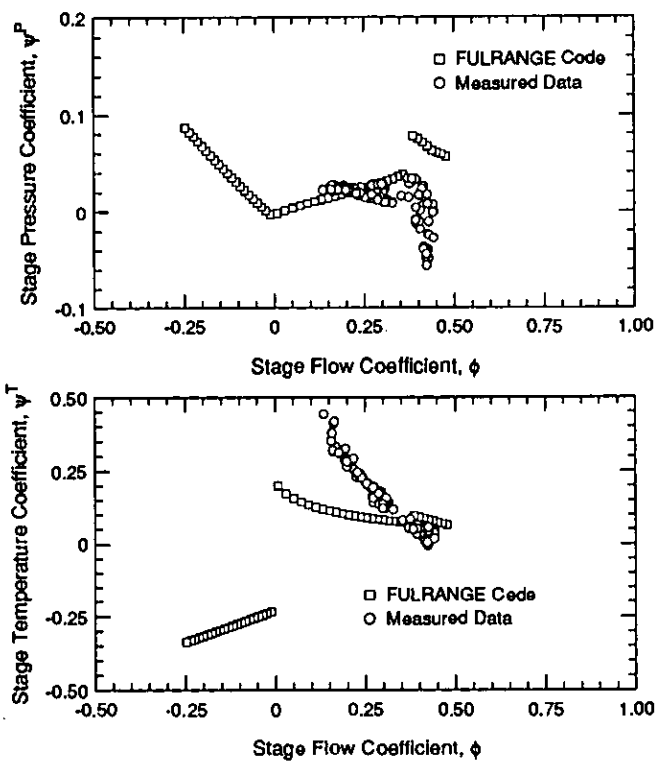

Fig. 10 10-Stage Compressor: a) Third Stage Pressure Characteristic; b) Third Stage Temperature Characteristic

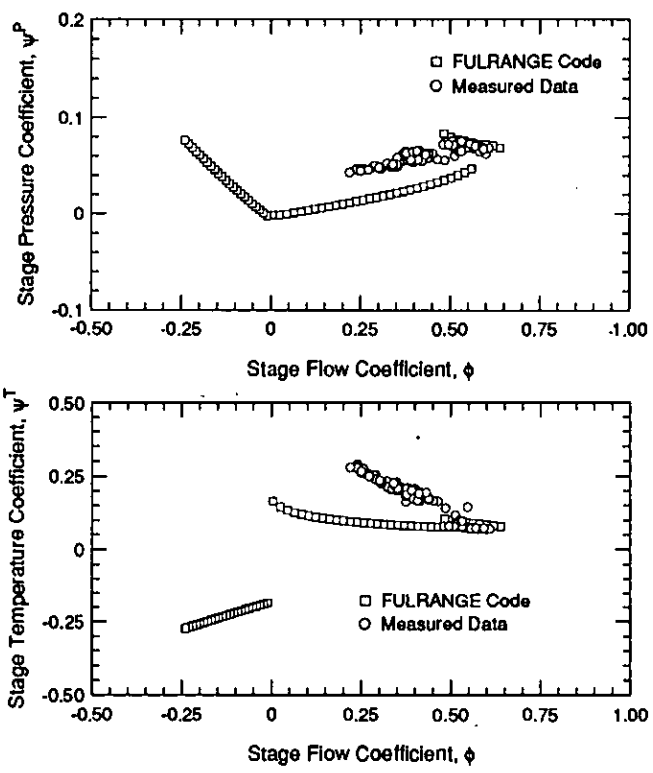

Fig. 11 10-Stage Compressor: a) Fifth Stage Pressure Characteristic; b) Fifth Stage Temperature Characteristic

Before discussing the reversed-flow pressure characteristics, it should be noted that the instrumentation placed on this compressor resulted in a stage being defined as a stator followed by a downstream rotor. There are two implications of this stage definition for reversed-flow operation. The first implication is that there is no "last stage stator" for which the losses should be neglected, because the tenth stator is not part of a stage for which performance was measured; the tenth stage consists of stator 9 and rotor 10. The second implication is that the effect of the fully closed IGV and first two stators in reversed flow will only be seen in the first and second stages; stator 3 will control the flow angle into stage 2, stator 2 will control the flow angle into stage 1, and flow downstream of the IGV in reversed flow is outside of the compressor.

Because of the experimental difficulty of generating reversed flow in high-speed, high-pressure ratio compressors, no reversed-flow data were obtained. For this compressor, the quantitative predictions of the model are therefore unsupported.

For similar stage geometries, Gamache (1985) measured nearly identical performance in reversed flow. The last eight stages of the 10-stage compressor were geometrically similar, and the reversed-flow performance predictions for these stages are very similar. The model predicted a smaller (magnitude) slope of the reversed-flow pressure characteristic for the first two stages because the IGV and first two stators are closed to the flow path. This resulted in a larger relative flow angle into the first and second rotors and more work being done on the air in the reversed direction.

Temperature Characteristic Predictions

The unstalled temperature predictions for the first three stages are higher than the measured characteristics, but show good qualitative agreement. It is believed that the errors in calculating the flow angles leaving the IGV and first two stators (which were fully closed to the flow path) resulted in the calculation of more flow turning than actually occurred. The predicted in-stall temperature rise for these stages is approximately correct at stall inception, but at lower mass flow the measured temperature rise increases much more than the present model predicts. This is believed to be the result of the significant viscous heating which occurs at low flow rates in high speed compressors.

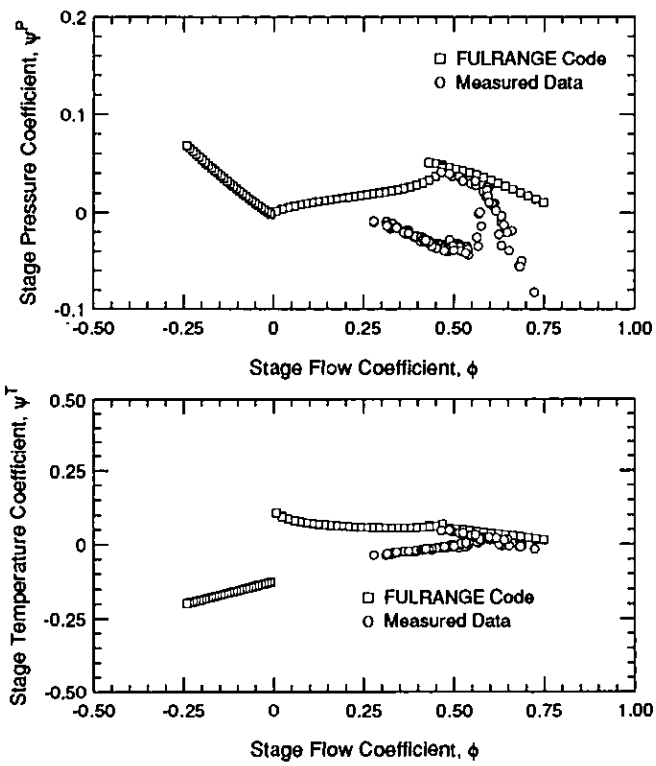

Fig. 12 10-Stage Compressor: a) Tenth Stage Pressure Characteristic; b) Tenth Stage Temperature Characteristic

At this time, an interesting point can be made about the perceived inception of stall. In the unstalled region, both the FULRANGE predictions and the measured temperature rise show a linear characteristic with negative slope. It is clear from the first and fifth stage data that the temperature characteristic experiences a discontinuous change in slope and curvature at the inception of stall (as defined by the slope of the pressure characteristic) and this is confirmed by the model. Since the change in slope of the measured temperature characteristic is much more pronounced than that of the pressure curve for these stages, it is suggested that temperature performance may be a better indicator of the onset of progressive stall. In reference to the performance of the second and third stages, the temperature characteristics would indicate that at flow coefficients less than 0.30 and 0.33, respectively, these stages are operating in-stall.

The unstalled temperature prediction for the fourth through tenth stages showed excellent agreement with the measured performance. A large fraction of the predictions are almost coincident with the data in this region. The in-stall predictions for the fourth and fifth stages show the same trend of under-predicted temperature rise at low mass flow that was shown by the first three stages, but this trend is less pronounced for the fourth stage.

The in-stall temperature predictions for the sixth through tenth stages are of the same form as for the first five stages (negatively sloped with positive concavity), but the measured characteristics are positively sloped and linear. The measured data often show a steady-state *drop* in temperature with an increase in pressure, which violates the second law of thermodynamics, for a portion of the stalled characteristic. Copenhaver (1988) suggested that the indicated drop in temperature was the result of significant recirculating flow within the rotating stall cells. As the flow moved backwards through each stage, work was done on it and its temperature increased.

For all stages, the reversed-flow temperature prediction is positively sloped and linear. The slope of the temperature characteristic is larger for the first two stages than for the last eight. This is because the IGV and first two stators are fully closed to the flow path, creating a larger relative flow angle to the rotor and resulting in higher turning. There are currently no reversed-flow data for this compressor, so comparisons cannot be made.

Finally, all of the above predictions must be viewed as the result of an axisymmetric model. The model cannot presently account for two- and three-dimensional, non-uniform effects which may influence the flow field.

CONCLUSIONS

A model has been developed for predicting wide range characteristics of axial-flow compressor stages, including in-stall and reversed flow. The model was applied to a 3-stage low-speed compressor, and very good agreement with the measured characteristics was shown. The prediction of the reversed-flow characteristics was essentially identical to the measured performance.

The model was applied to a 10-stage high-speed compressor and mixed results were shown. There were effects of compressibility apparent in the forward stages which could not be captured by the current model. The predicted pressure characteristics showed very good agreement with the unstalled performance of the last five stages, although the tenth stage characteristics diverged at high mass flows. The in-stall prediction was positively sloped and similar for all stages, but the measured performance was dependent on the stage location; the measured slopes were positive for some stages and negative for others. The reversed-flow pressure characteristics are in good qualitative agreement with those of the low-speed compressor modeled, but no high-speed data exists in the open literature for this flow regime.

The unstalled temperature predictions for the first three stages showed the correct trends, but were larger than the measured performance; for the last seven stages, the agreement was excellent in this flow regime. At low flow rates, the model under-predicted the temperature rise for the first five stages by a substantial amount; it is

believed that this is the effect of significant viscous heating which is not captured by the present model. The in-stall performance of the last five stages indicated a significant amount of recirculating flow in the rotating stall cells which could not be predicted by the steady-state, mean-line stage model.

As mentioned previously, the unstalled temperature predictions for the ninth and tenth stages were very close to the measured values, but the pressure characteristics did not show the same level of agreement. It is suggested that the stage losses, and hence the performance, are a function of the environment in which the stage is operated, as well as the aerodynamic design of the stage.

The stage temperature characteristic is essentially linear in the unstalled operating region, but has a discontinuous change in slope and curvature at the inception of progressive stall. Because a stage can operate in-stall with a negatively sloped pressure characteristic, it is suggested that the temperature characteristic might be a better indicator of stall inception.

When a stage stalls, it upsets the flow field downstream to a sufficient extent that it can drive the next downstream stage into stall, even if the downstream stage was operating away from its stall point. It is also possible that choking of a downstream stage can prevent upstream stages from operating at higher mass flows which might be attainable if the upstream stages were operated in isolation. For these reasons, it is suggested that there are certain points on the steady-state stage characteristics which cannot be reached in a multi-stage environment. This is complimentary to the conclusion that a stage operated in a multi-stage environment could operate unstalled at flows significantly below the isolated clean-flow stall point, as reported by Longley and Hynes (1990).

ACKNOWLEDGEMENTS

Portions of the reported work were supported by the Joint Dynamic Airbreathing Propulsion Simulations (JDAPS) program of the U.S. Air Force and U.S. Army.

REFERENCES

Boyer, K. M., and O'Brien, W. F., 1989, "Model Predictions for Improved Recovery of a Multistage Axial-Flow Compressor," AIAA Paper No. 89-2687.

Carneal, J. P., 1990, "Experimental Investigation of Reversed Flow in a Compressor Cascade," *M.S. Thesis*, V.P.I.&S.U., Blacksburg, VA.

Cousins, W. T., 1991, Private Communication, V.P.I.&S.U., Blacksburg, VA.

Davis, M. W., 1986, "A Stage-by-Stage Post-Stall Compression System Modeling Technique: Methodology, Validation, and Application," *Ph.D. Dissertation*, V.P.I.&S.U., Blacksburg, VA.

Dixon, S. L., 1975, *Fluid Mechanics, Thermodynamics of Turbomachinery*, Pergammon Press.

Dowler, C. A., Boyer,K. M., and Poti, N., 1989, "Model Predictions of Fan Response To Inlet Temperature Transients and Spatial Temperature Distortion," AIAA Paper No. 89-2686.

Gamache, R. N., 1985, "Axial Compressor Reversed Flow Performance," *Ph.D. Dissertation*, M.I.T., Cambridge, MA.

Graham, R. W., and Guentert, E. C., 1965, "Compressor Stall and Blade Vibration," Chapter XI of *Aerodynamic Design of Axial Flow Compressors*, Johnson, I. A., and Bullock, R. O., eds., NASA SP-36.

Greitzer, E. M., 1976, "Surge and Rotating Stall in Axial Flow Compressors, Part I: Theoretical Compression System Model," ASME *Journal of Engineering for Power*, pp. 190-198.

Horlock, J. H., 1973, *Axial Flow Compressors*, Robert E. Krieger Publishing Company.

Kimzey, W. F., 1977, "An Analysis of the Influence of Some External Disturbances on the Aerodynamic Stability of Turbine Engine Axial Flow Fans and Compressors," Arnold Engineering Development Center TR-77-80.

Koch, C. C., and Smith, L. H., 1976, "Loss Sources and Magnitudes in Axial-Flow Compressors," ASME *Journal of Engineering for Power*, pp. 411-424.

Koff, S. G., and Greitzer, E. M., 1986, "Axisymmetrically Stalled Flow Performance for Multistage Axial Compressors," ASME *Journal of Turbomachinery*, pp. 216-223.

Lieblein, S., 1959, "Loss and Stall Analysis of Compressor Cascades," Transactions of the ASME, *Journal of Basic Engineering*, pp. 387-400.

Lieblein, S., 1965, "Experimental Flow in Two-Dimensional Cascades," Chapter VI of *Aerodynamic Design of Axial Flow Compressors*, Johnson, I. A., and Bullock, R. O., eds., NASA SP-36.

Longley, J. P., and Hynes, T. P., 1990, "Stability of Flow Through Multistage Axial Compressors," ASME *Journal of Turbomachinery*, pp. 126-132.

Moses, H. L., and Thomason, S. B., 1986, "An Approximation for Fully Stalled Cascades," ASME *Journal of Propulsion*, pp. 188-189.

Saravanamuttoo, H. I. H., and Fawke, A. J., 1970, "Simulation of Gas Turbine Dynamic Performance," ASME Paper 70-GT-23.

Seldner, K., Mihaloew, J. R., and Blaha, R. J., 1972, "Generalized Simulation Technique for Turbojet System Analysis," NASA TN D-6610.

Tumer, R. C. and Sparkes, D. W., 1964, "Complete Characteristics For a Single-Stage Axial-Flow Fan," Thermodynamics and Fluid Mechanics Convention, *Proceedings of the Institution of Mechanical Engineers*, Cambridge, England.

Yocum, A. M. II, 1988, "An Experimental and Numerical Investigation of the Performance of Compressor Cascades With Stalled Flow," *Ph.D. Dissertation*, V.P.I.&S.U., Blacksburg, VA.

APPENDIX A

Stationary cascade data can be expressed in terms of a wheel speed, U, for a rotating cascade by assuming that the relative velocity in the rotating cascade is the measured test velocity in the stationary cascade. Referring to Fig. 4, for the rotor in reversed flow, the relative velocity, W_2, is equivalent to the cascade test velocity. Define

$$V_{x2} = W_2 \cos\beta_2 \tag{20}$$

$$\beta_2 = \alpha - \gamma \tag{21}$$

where α is the angle of attack of flow into the cascade and γ is the cascade stagger angle. Since the original cascade data (Carneal, 1990) were reported in terms of W_2, α, and γ, Equations (20) and (21) define V_{x2} and β_2. From the geometry of Fig. 4,

$$U = W_2 \sin\beta_2 - V_{x2} \tan\alpha_2 \tag{22}$$

To close the system of equations, Carneal (1990) assumed an absolute flow angle, α_2, of 45°, the approximate value of the reversed-flow stator discharge angle for the last stage of a low-speed compressor to which comparisons were made. Given the limited data and the approximate nature of the reversed-flow loss estimates, the low-speed loss curve was used to develop predictions for the high-speed compressor, which had similar reversed-flow stator discharge angles. Thus, from the original stationary cascade data, an equivalent rotor inlet value of V_x/U may be determined.

The stationary cascade losses were reported in terms of a mixed-out loss coefficient,

$$\overline{\omega}_3 = \frac{\Delta P_0}{\frac{1}{2}\rho W_2^2} \tag{23}$$

To express the losses in terms of wheel speed, define

$$\overline{\omega}_{3corr} = \overline{\omega}_3 \left(\frac{W_2^2}{U^2}\right) \tag{24}$$

Fig. 5 is the result of the application of these transformations.